Atomic Structure of Adenosine Deaminase Complexed with a Transition-State Analog: Understanding Catalysis and Immunodeficiency Mutations

DAVID K. WILSON, FREDERICK B. RUDOLPH, FLORANTE A. QUIOCHO*

The crystal structure of a murine adenosine deaminase complexed with 6-hydroxyl-1,6-dihydropurine ribonucleoside, a nearly ideal transition-state analog, has been determined and refined at 2.4 angstrom resolution. The structure is folded as an eight-stranded parallel α/β barrel with a deep pocket at the β-barrel COOH-terminal end wherein the inhibitor and a zinc are bound and completely sequestered. The presence of the zinc cofactor and the precise structure of the bound analog were not previously known. The 6*R* isomer of the analog is very tightly held in place by the coordination of the 6-hydroxyl to the zinc and the formation of nine hydrogen bonds. On the basis of the structure of the complex a stereoselective addition-elimination or S_N2 mechanism of the enzyme is proposed with the zinc atom and the Glu and Asp residues playing key roles. A molecular explanation of a hereditary disease caused by several point mutations of an enzyme is also presented.

ADENOSINE DEAMINASE (ADA), A KEY ENZYME IN PURINE metabolism, catalyzes the irreversible hydrolysis of adenosine or deoxyadenosine to their respective inosine product and ammonia. It is present in virtually all mammalian cells and has a central role in maintaining immune competence. Lack of the enzyme is associated with severe combined immunodeficiency disease (SCID) [see (*1*) for reviews], which makes ADA a paradigm for structure-function studies of a genetic disease. The first clinical trial of gene therapy is being carried out on a patient with SCID caused by a defect in the ADA gene. ADA is also specifically involved or its levels are changed in a variety of other diseases including acquired immunodeficiency syndrome, anemia, various lymphomas, and leukemias (*2*).

The levels of ADA have been shown to be high in developing T cells, the stomach and intestine, and the fetal-maternal interface (*3*), which suggests roles related to the growth rate of cells and embryo and to implantation (*4*). The function of ADA is also critical in controlling the effects of adenosine in a variety of systems. Adenosine is an endogenous anticonvulsant and antihypoxic and a modulator of blood flow, platelet aggregation, lipolysis, glycogenolysis, and neurotransmission (*5*).

ADA is also a well-studied model for catalytic function through binding of numerous inhibitors, including ground-state and very potent transition-state analogs. Some of the inhibitors of ADA are used, alone or in combination with other drugs, as antimetabolic, antineoplastic, and antibiotic agents (*6*). The reaction catalyzed by ADA appears to be encounter limited with a rate enhancement of $\sim 10^{12}$ (*7*). All previous studies have suggested that no bound cofactors were required for activity (*8*). The mechanism of ADA is thought to be of the addition-elimination type with the direct addition of water to the C-6 position of the purine ring, which would result in the formation of a tetrahedral intermediate (*9*).

Structure determination and structure of ADA. Crystals of the murine ADA were obtained at pH 4.2 from a solution of the enzyme (15 mg/ml) and 25 mM purine ribonucleoside (Sigma Chemical) by a procedure similar to that used in the crystallization of the complex of ADA with 2′-deoxycoformycin (*10*). [The enzyme was purified from an *Escherichia coli* strain that contained a plasmid with the cloned gene for murine ADA (*11*).] Crystals were harvested in a solution containing saturated (~200 mM) purine ribonucleoside. The crystals have *C*2 space group, unit cell dimensions of a = 102.36 Å, b = 94.11 Å, c = 72.93 Å, and β = 127.19°, and a solvent content of ~65 percent that was exploited in the improvement of phases by density modification in the structure determination. Diffraction intensities were measured at 4°C with an ADSC two-area detector system mounted on a Rigaku RU-200 rotating anode. Only one crystal was required for each diffraction data set (Table 1).

Initial 3 Å phases, which produced electron density maps that enabled us to trace the polypeptide backbone, were obtained by multiple isomorphous replacement (MIR) from three derivatives (one site from *p*-chloromercuriphenyl sulfonic acid, two sites from mercuriphenylglyoxal, and two sites from potassium platinum tetranitrate) together with anomalous scattering contributions from the two mercury derivatives. Application of phase improvement algorithms (*12*) to the MIR-anomalous phases improved the overall figure of merit from 0.63 to 0.82 at 3.0 Å resolution, which permitted verification of the polypeptide chain trace and fitting of the amino acid sequence (*13*). The crystal structure was subsequently refined for 20,445 native reflections between 10 and 2.4 Å

D. K. Wilson and F. A. Quiocho are in the Howard Hughes Medical Institute and the Department of Biochemistry, Baylor College of Medicine, Houston, TX 77030. F. B. Rudolph is in the Department of Biochemistry and Cell Biology, Rice University, Houston, TX 77005.

*To whom correspondence should be addressed.

resolution with the use of molecular dynamics and restrained refinement [program XPLOR (*14*)] to a final crystallographic *R* factor of 0.19 (Table 1) (*15*).

ADA contains a parallel α/β-barrel motif with eight central β strands and eight peripheral α helices (Fig. 1), which is similar to the structure previously observed in 17 other enzymes (*16*). The structure has five additional helices. The long peptide segments (residues 19 to 76) located between β1 and α1 folds into a loop of three helices (identified as H1, H2, and H3 to distinguish them from the helices of the barrel). Following α8, the polypeptide chain terminates into two antiparallel COOH-terminal helices (H4 and H5) that lie across the NH_2-terminal of the β barrel (Fig. 1C). The residues associated with the β barrel, including those in the ligand-loaded active site located at the β-barrel COOH-terminal end, exhibit temperature factors that are generally lower than those of the peripheral helices connecting the strands (Fig. 1A). During the course of refining the structure we discovered that the active site also contains a bound metal.

The structure of the bound ligand. Purine ribonucleoside (compound **II**, Fig. 2) is considered to be a substrate or "ground-state" analog with an apparent inhibition constant K_i of 2.8×10^{-6} M (*17*). Although crystals of ADA were obtained and stored in solutions containing high excess concentration of **II**, there was an uncertainty as to the actual species bound. Carbon-13 nuclear magnetic resonance and ultraviolet spectral measurements suggested that purine ribonucleoside is bound in a form that is tetrahedral (sp^3) at the C-6 position (*18*). The bound form could either be the extremely rare species of purine ribonucleoside that is hydrated at the N-1 and C-6 positions (*19*) or a covalently bonded complex formed by the addition of an active site sulfur or oxygen nucleophile at the active site (*18*). The rare hydrated species, 6-hydroxyl-1,6-dihydropurine ribonucleoside (HDPR), is thought to be a nearly ideal transition-state analog with an estimated affinity ($K_i = \sim 10^{-13}$ M) that exceeds those of substrates, products, and **II** by factors greater than 10^8 (*19*). Neither the hydrated species nor the covalently bonded complex has been unambiguously proven to exist.

Although the density of a bound ligand in electron density maps was evident even before structure refinement was initiated, it was only after an *R* factor of ~0.25 was attained in the XPLOR refinement at 2.4 Å resolution that the model of the purine ribonucleoside was fitted with ease to a $(2|F_o| - |F_c|, \alpha_c)$ map. After two additional rounds of refinements, which reduced the *R* factor to 0.22 and led to the identification of a metal ion and all ordered water molecule in the ligand-binding site, a $(|F_o| - |F_c|, \alpha_c)$ difference map revealed a significant well-resolved density peak that was within covalent distance and in axial position of the C-6 of the purine ribonucleoside. This provided a solid structural clue that the bound ligand is the hydrated species of the purine ribonucleoside. Resumption of the refinement with the model of the ribonucleoside modified to include an axial hydroxyl group covalently bonded to C-6 ultimately yielded the difference electron density shown in Fig. 3A. The structure refinement result provides direct evidence that HDPR is bound and apparently stable within the confines of the active site. It also shows unambiguously that the 6*R* diastereomer of HDPR (compound **III**, Fig. 2) is recognized preferentially by ADA (Fig. 3B). Although HDPR (**III**) is considered an extremely rare component of the purine ribonucleoside (**II**), the result suggests an equilibrium shift between **II** and **III** in the presence of ADA to yield saturating amount of **III**. Our results also raise the possibility that ADA carries out the stereospecific hydration of the purine ribonucleoside to produce a sufficient amount of the "pseudo-suicide" HDPR analog.

Zinc coordination. As ADA has been previously shown to require no cofactor (7), the presence of a metal in the structure was surprising. Adenosine monophosphate deaminase, which catalyzes a similar hydrolytic deamination reaction, has been shown to be inactivated by *o*-phenanthroline, a zinc-specific chelating agent (7).

As the density of the metal and the nature of its coordination were very suggestive of a bound zinc, a zinc atom was included in the structure refinement. After completion of the structure refinement, attaining a *B* factor of the metal consistent with a bound zinc, independent metal analysis by atomic absorption spectroscopy of three samples of ADA indicated 0.9 ± 0.1 zinc atom bound per enzyme molecule. The enzyme is also susceptible to inhibition at pH 5.0 by *o*-phenanthroline and dipicolinic acid (*20*).

The zinc ion, which lies in the deepest part of the active site pocket (Fig. 1C), is coordinated by five atoms—three Nε2 atoms of His^{15}, His^{17}, and His^{214}, the Oδ2 of Asp^{295}, and the O-6 of HDPR (Fig. 3B and Table 2). The three Nε2 atoms exhibit tetrahedral geometry with Oδ2 and O-6 sharing the remaining site.

Atomic interactions between ADA and HDPR. The deep oblong-shaped active site cavity or pocket is lined by the COOH-terminal segments and connecting loops of the β-barrel strands (Fig. 1). The purine unit of HDPR, which is above the zinc, is in a more enclosed area, whereas the ribose group is closer to the opening of the pocket (Fig. 1). The narrow opening of the cavity is partially capped on one side by H3 helix (residues 58 to 67) and on the opposite side by a loop (residues 183 to 188) between β3 and α3 (Fig. 1). The H3 helix contains several hydrophobic residues hanging over the purine ring of HDPR.

The major features of the polar interaction between ADA and HDPR are shown in Fig. 3. The bound HDPR is in the anti-conformation (Fig. 3, A and C) that is commonly observed for nucleosides. For convenience, we have identified the two surfaces of the purine rings as A-face and B-face in which the numbering of the pyrimidine ring (Fig. 2) increases in a clockwise and counterclockwise direction, respectively. The plane of the purine is almost perpendicular to the β barrel, with the B-face directed toward the bot-

Table 1. Crystallograhic and refinement data. Abbreviations: PCMB, *p*-chloromercuriphenyl sulfonic acid; HGPG, mercuriphenylglyoxal; PTNO, potassium platinumtetranitrate; HDPR, 6-hydroxyl-1,6-dihydropurine riboside; and rms, root mean square. Definitions: *R* merge is the *R* factor on intensities for merging symmetry-related reflections; *R* Cullis = $\Sigma||F_{PH} \pm F_P| - |F_H||/\Sigma|F_{PH} - F_P|$; where the structure factors are for the protein (F_P), the heavy atom (F_H), or their complex (F_{PH}); *R* anom (rms) = $[\Sigma(\Delta F^{\pm}{}_o - \Delta F^{\pm}{}_c)^2/\Sigma(\Delta F^{\pm}{}_o)^2]^{1/2}$, where F_o is the observed and F_c is the calculated structure factors; and *R* factor = $\Sigma|F_o - F_c|/\Sigma|F_o|$.

Parameter	Native	PCMB	HGPG	PTNO
Resolution limit	2.4	3.0	3.0	4.0
Reflections				
Measured	72,059	50,220	42,703	17,454
Unique	20,445	9,823	8,764	3,525
R merge	3.24	4.30	6.79	4.88
Phasing statistics				
f_H/residual		1.17	0.96	0.72
R Cullis		0.76	0.76	0.91
R anom (rms)		0.55	0.65	
Refinement statistics				
R factor	0.195			
Protein atoms	2,792			
HDPR atoms	19			
Zinc atom	1			
Ordered waters	58			
Deviation (rms) from ideal bond distance (Å)	0.003			
Deviation (rms) from ideal angle (°)	1.366			

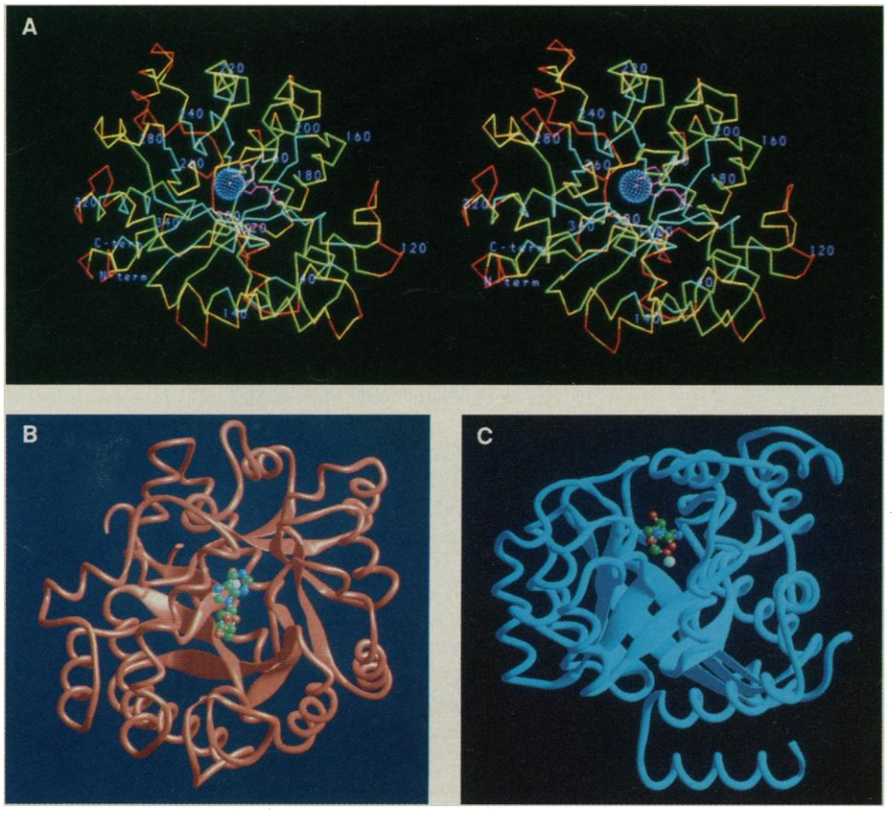

Fig. 1. The backbone trace of the refined 2.4 Å structure of the adenosine deaminase (ADA). (**A**) Stereoscopic view of the α-carbon backbone down the COOH-terminal end of the β barrel. Every twentieth α-carbon is numbered, and N term and C term designate the NH_3 and COOH terminal ends, respectively. The α-carbons are colored according to their refined temperature factors: blue, B values of between 5 and 10 Å^2; green, between 10 Å^2 and 15 Å^2; yellow, between 15 Å^2 and 20 Å^2; orange, between 20 Å^2 and 25 Å^2; and red, greater than 25 Å^2. The 6-hydroxyl-1,6-dihydropurine ribonucleoside (HDPR) (orange color) and zinc ion (with van der Waals dot surface) are bound in the deep pocket located at the COOH-terminal end of the β barrel. CHAIN (*41*), a program developed by J. Sack in our laboratory, was used in the molecular modeling, density fitting, and displaying of structures. (**B**) Perspective view of the polyglycine backbone trace (down the COOH-terminal end of the β barrel) with the bound HDPR (ball and stick model) and zinc (white) below the purine ring of HDPR. (**C**) Identical structure as in (B) but perpendicular to the β barrel. Note the deep active site pocket containing the HDPR and zinc and the two peptide segments (residues 58 to 67 and residues 183 to 188) hanging above the HDPR and forming partial "lids" of the pocket. (B) and (C) were obtained by the RIBBON program of M. Carson (*41*).

tom of the pocket and the A-face toward the cleft opening (Fig. 1).

In addition to the coordination of the 6-hydroxyl group to the zinc, HDPR is held in place by nine hydrogen bonds with seven residues, of which five have polar planar side chains. Surprisingly, four of the side chains have carboxyl groups—Asp^{19}, Glu^{217}, and Asp^{296}.

The carboxyl group of Glu^{217} is roughly coplanar with the purine ring and its Oδ1 is in a position to accept a hydrogen bond from N-1 of HDPR and to interact with an ordered water molecule. The carboxyl group is within van der Waals distance of Leu^{58}, Thr^{269}, and Val^{218}, suggesting a higher pK_a (acidity constant) than normal.

The close proximity of the carboxyl moiety of Asp^{296}, which is almost perfectly coplanar with the purine ring, to the N-7 also indicates a hydrogen-bonding interaction. As the carboxyl group is in a highly hydrophobic environment, and makes van der Waals contacts with three Phe residues (61, 65, and 300), it is likely to remain protonated at higher pH and, hence, serves as the hydrogen-bond donor. The N-3 of HDPR accepts a hydrogen bond from the NH group of Gly^{184}.

Of the active site residues, Asp^{296} makes the most extensive interactions that are indicative of an ionized carboxylate group. The Oδ2 provides one of the ligands to the Zn^{2+} while the Oδ1 accepts hydrogen bonds from the 6-OH of HDPR and the γ-OH of Ser^{265} and forms a salt link with His^{238}. His^{238}, which we consider to be positively charged because of its proximity to Asp^{295}, donates a hydrogen bond to the 6-OH of HDPR.

The ribose, with a $C_{3'}$-*endo* pucker, is engaged in six hydrogen bonds, four with two side chains and two with an ordered water molecule. The 3′-hydroxyl donates a hydrogen bond to Oδ2 of Asp^{19}. The 5′-OH forms a bifurcated hydrogen bond with Oδ1 and Oδ2 of Asp^{19} and further accepts a hydrogen bond from Nδ1 of His^{17}, whose Nε2 is coordinated to the zinc. An ordered water molecule is within hydrogen-bonding distance of the 2′-hydroxyl, which projects towards the opening of the cavity, and the 3′-hydroxyl.

The stereoselectivity of ADA for the 6*R* isomer of HDPR, a feature very much relevant to the catalytic mechanism of ADA (described below), is strictly governed by the location of the triad of zinc ion, Asp^{295}, and His^{238} on the B-face side of the purine ring (Fig. 3, A to C). Interestingly, whereas the B-face of the purine ring is exposed to polar groups and the zinc, the A-face sees nothing but nonpolar residues composed of Leu^{58}, Phe^{61}, Leu^{62}, and Phe^{65} lodged in one of the segment (residues 58 to 67) capping the active site pocket (see above and Fig. 1).

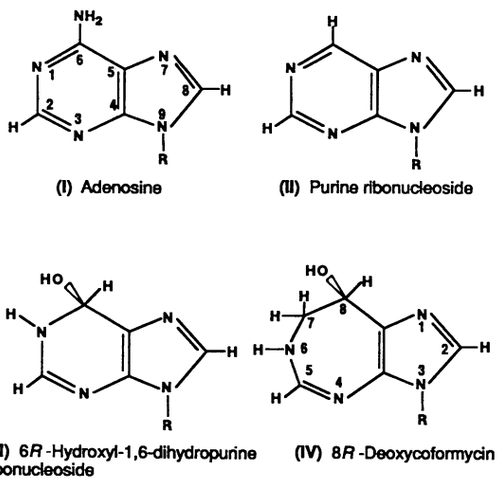

Fig. 2. Structures of the substrate and inhibitors of ADA. The R sugar unit in compound I to III is ribose, while in compound IV is 2′-deoxyribose. The 6*R* isomer of compound III and 8*R* isomer of IV are shown.

Ligand-induced conformational change. The HDPR molecule is almost completely inaccessible to solvent; based on the Lee and Richards criteria (*21*), the solvent accessible surface of HDPR in the free state (76 Å^2) is reduced to 0.5 percent when bound in the active site pocket. This difference indicates that a structural change occurs in order for the sequestered HDPR to dissociate from the pocket. The existence of two loops (residues 58 to 67 and residues 183 to 188) that form partial "lids" of the pocket (Fig. 1) and contain residues that contact HDPR suggests a possible mechanism for the structural change. A movement of one or both lids in the "open" form would allow access to and from the site. This type of conformational change has been observed in triose phosphate isomerase, the first enzyme found to have the β-barrel motif and a buried active site cavity at COOH-terminal end of the β barrel (*22*).

Binding of substrate and other transition-state analogs. The structure of ADA complexed with the transition-state analog provides an excellent framework for the molecular understanding of the binding of substrates and other potent inhibitors as well as the mechanism of the enzyme. Since leaving groups at the C-6 position other than the amino group (such as F, Cl, and methoxy) are permitted (*8, 18*), it makes no significant contribution to ligand specificity. The molecular determinants crucial for the substrates of ADA are consistent with the mode of binding of HDPR (Fig. 3). The presence of lone pairs in both N-3 and N-7 of adenosine are necessary for binding as evidenced by the observation that 3- or 7-deazaadenosine is neither a substrate nor a tightly bound inhibitor (*23*). The finding that 1-deazaadenosine is tightly bound (K_i = 2 μM) but not deaminated (*23*) indicates that N-1 with a lone pair is critical for substrate turnover. The ribose unit is also catalytically important as indicated by the finding that, while adenosine and adenine have similar values of Michaelis constant (K_m), the former is deaminated ~10^4 faster than the latter (*8, 23, 24*). As can be seen in the ADA-HDPR structure, the 2′-hydroxyl is not essential. Indeed, 2′-deoxyadenosine is as good a substrate as adenosine (*8*).

Coformycin and 2′-deoxycoformycin (compound **IV**, Fig. 2) were the first compounds to be discovered as potent transition-state inhibitors of ADA—K_i values of about 10^{-8} and 10^{-12} M, respectively (*9, 25*). The potency of these compounds is dependent

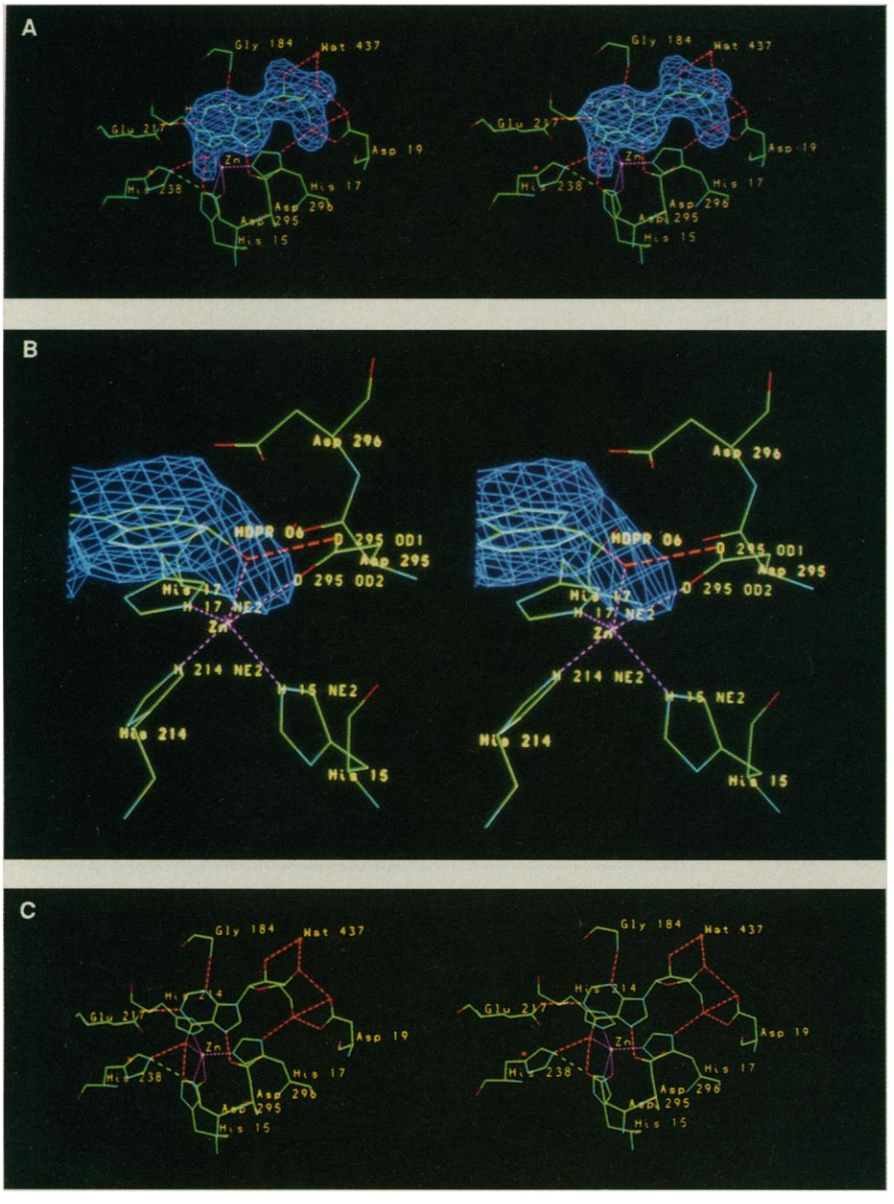

Fig. 3. Polar interactions between ADA and HDPR and the zinc ion. (**A**) Stereo view of the electron density surface (blue) of the HDPR and superimposed refined structure of the active site. The density map was calculated with coefficients ($|F_o| - |F_c|$) and α_c phases calculated from the refined structure with the contribution of the HDPR model omitted. The difference density is contoured at 3σ of the electron density and a grid spacing of 0.8 Å. Hydrogen bonds are represented by red dashed lines and zinc coordination by magenta dashed lines. (**B**) A close-up stereo view of the coordination of the zinc and the 6 *R*-hydroxyl conformation of HDPR. Atoms are color coded as follows: oxygen, red; nitrogen, blue; and carbon, green. (**C**) Identical to (A), with the difference electron density removed for clarity. (**D**) Schematic diagram of the interaction between ADA and HDPR. Numbers near dashed lines indicate distances (in angstroms) between interacting atoms. As discussed in the text, Glu^{217} and Asp^{296} are likely to have pK_a values greater than normal, His^{238} and Asp^{295} are likely to be in the ionized or charged species, and His^{17} (a zinc ligand) is neutral.

on the stereochemisty at the hydroxyl-bearing C-8 position; the 8*R* isomer of **IV** (Fig. 2) binds ~10^7 times more strongly than the 8*S* isomer (*26*). This finding is in complete accord with the stereoselectivity of ADA for the 6*R* of HDPR (see above). In contrast, the hydroxyl group of *S*-isomers of the analogs, including HDPR, would be projecting not only away from the zinc, Asp^{295}, and His^{238} but also into an area surrounded by the hydrophobic residues Leu^{58}, Phe^{61}, Leu^{62}, and Phe^{65}.

How do we account for the very tight binding of the potent transition-state analog inhibitors? Kati and Wolfenden (*19*) have attributed the approximately −10 kcal/mol contribution of the 6-hydroxyl to the free energy of binding of HDPR to a single hydrogen bond between the hydroxyl and an unidentified charged Asp or Glu residue. Such a strength for one hydrogen bond of this type is unprecedentedly high. Monosaccharides that are completely sequestered in protein binding sites and bound by 10 to 13 cooperative hydrogen bonds formed between five sugar hydroxyl groups and mostly charged residues (such as Asp and Glu) have, at best, a total binding energy of about −9 kcal/mol (*27*). On the basis of the structure of the ADA-HDPR complex, we believe that the coordination of the 6-hydroxyl of HDPR to the zinc imparts the greatest stability to the complex.

Catalytic mechanism. In light of the atomic interaction between ADA and HDPR, we propose a stereospecific addition-elimination (with a tetrahedral intermediate) or S_N2 mechanism of ADA shown in Fig. 4. In either mechanism, Asp^{295} acts as a general base and the zinc serves as a powerful electrophile to activate the water molecule. His^{238} further assists in orienting the water and stabilizing the charge of the attacking incipient hydroxide. The protonated Glu^{217} or the water hydrogen bonded to it could donate or share a proton with N-1 of the substrate.

The stereospecificity of the chemical reaction is conferred by the location of the zinc, Asp^{295}, and His^{238} on the B-face side of the purine ring. [Water attack on the A-face side is less likely because the only residues on this side have apolar side chains (see above).] This specificity indicates that the axial–NH_2 leaving group on the A-face side would be favorably directed toward the narrow opening of the cleft.

The lack of a proton donor group close to the A-face side of the purine casts an uncertainty as to the origin of the proton for the ammonia leaving group that would be projecting from this side. Model building of an axial NH_2 on the C-6 of HDPR indicates that the closest sources of a proton are Asp^{295}, which would have the proton abstracted from the water, and the positively charged His^{238} If His^{238} acts as the proton donor, its proximity to the general base Asp^{295} could facilitate reprotonation.

Because of the possibility that the axial –NH_2 or other polar leaving groups would be located in an unfavorable hydrophobic environment (see above), the tetrahedral intermediate may be extremely short-lived. Therefore, an S_N2 mechanism in which water addition and ammonia elimination occur more or less synchronously (**1** directly to **3** in Fig. 4) is a strong alternative to the addition-elimination mechanism.

The involvement of every nitrogen lone pair of adenosine in hydrogen-bonding interactions should further enhance catalysis by reducing the aromaticity of the purine ring and thereby making the C-6 more susceptible to attack by water. It also facilitates any distortion of the pyrimidine ring in order to accommodate the transformation of N-1 and C-6 from sp^2 to sp^3 in the tetrahedral intermediate. Moreover, since the pK_a values of N-1, as well as the other purine nitrogens, and the carboxyl side chain are not too greatly different, protonation of N-1 would be more facile even under the influence of the environment in the active site.

Some of the features of the ADA mechanism, especially the involvement of a zinc ion and a carboxylate residue in promoting the nucleophilic attack by a water molecule, bear strong similarity with the proposed mechanisms of peptide hydrolysis by carboxypeptidase A (*28*) and thermolysin (*29*). The proposed dual role of the zinc in ADA—aligning the carboxylate residue and activating the attacking water molecule—is a new wrinkle in the mechanism of a zinc enzyme catalyzing a hydrolytic reaction.

Addition-elimination (*9, 19, 30*) and double-displacement (*8, 18, 31*) mechanisms of ADA have been previously proposed, but the only residue, a cysteine, that has been widely considered to play an important role in either mechanism is not close to N-1 and C-6 of the bound HDPR. A thiol group has been proposed to be a donor in the protonation of N-1 in the addition-elimination mechanism (*19, 30, 32*) or a nucleophile in the direct attack of C-6 in the double-displacement mechanism (*8, 18, 31*). Of the five Cys residues, two (Cys^{153} and Cys^{262}) are close to the active site pocket. The γ-SH of Cys^{262} is the closest to N-1 (7.9 Å) and C-6 (7.3 Å) of HDPR, respectively. Not only are these distances too far for the thiol group to play a direct role, but access by the thiol to the active

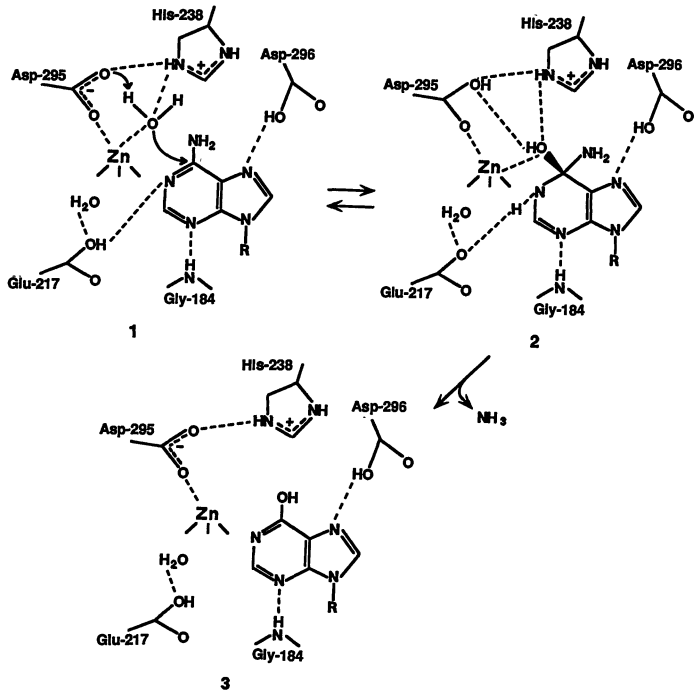

Fig. 4. Proposed addition-elimination or S_N2 catalytic mechanism of ADA. See text for description. The addition-elimination mechanism assumes the formation of a tetrahedral intermediate **2**. The S_N2 mechanism proceeds from **1** directly to **3** in synchrony with the elimination of NH_3. The origin of the proton for the ammonia leaving group is discussed in the text.

Table 2. Zinc coordination in ADA.

Coordination	Distance (Å)	Coordination	Angle (°)
Nε2 (His^{15})---Zn	2.3	Nε2 (15)---Zn---Nε2 (17)	109.1
Nε2 (His^{17})---Zn	2.1	Nε2 (15)---Zn---Nε2 (214)	93.9
Nε2 (His^{214})---Zn	2.2	Nε2 (15)---Zn---Oδ2 (295)	79.4
Oδ2 (Asp^{295})---Zn	2.4	Nε2 (15)---Zn---O-6 (HDPR)	127.2
O-6 (HDPR)---Zn	2.3	Nε2 (17)---Zn---Nε2 (214)	105.9
		Nε2 (17)---Zn---Oδ2 (295)	86.4
		Nε2 (17)---Zn---O-6 (HDPR)	113.9
		Nε2 (214)---Zn---Oδ2 (295)	167.5
		Nε2 (214)---Zn---O-6 (HDPR)	102.2
		Oδ2 (295)---Zn---O-6 (HDPR)	74.3

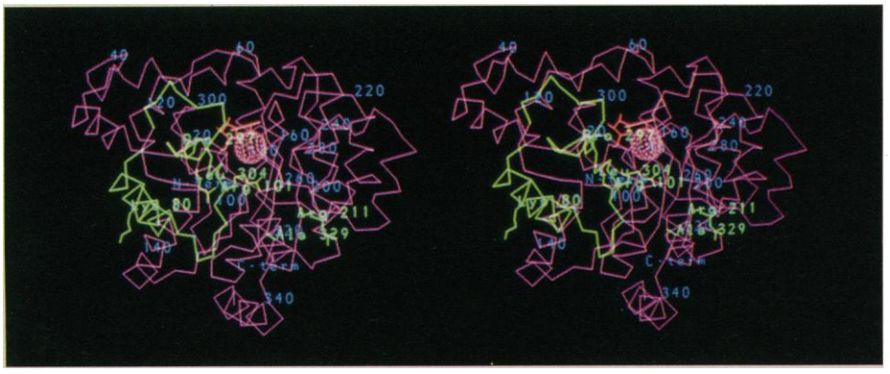

Fig. 5. Stereo view of the α-carbon trace (magenta color) of ADA showing the bound HDPR (red), zinc (van der Waals dot surface), and residues and segment that undergo mutations in five cell lines (Table 3) derived from patients with ADA deficiency.

site is prevented by a wall of residues consisting of His^{238}, Ser^{265}, and Asp^{295}, which are themselves intimately associated with the active site. Although the γ-SH of Cys^{153} is within 4 Å of the C-5′ of the ribose unit, it is at a much farther distance (~9 Å) and directed away from N-1 and C-6.

The structure of the ADA complexed with the transition-state analog has little to offer in support of a double-displacement mechanism. This mechanism has also been considered unlikely on other grounds (*19, 32*), including the finding that ADA catalyzes the hydration of pteridine (*33*). Hydration of the pteridine can occur stereospecifically by way of either of the mechanisms described herein.

Chang *et al.* (*30*) have compared the amino acid sequences of the human, murine, and *E. coli* ADA. We observe that the essential residues in the active site of the murine ADA structure (including the residues that coordinate the zinc), are conserved in the human and *E. coli* ADA and comparison to the sequence of adenosine monophosphate deaminase suggests similar reaction mechanism for both enzymes.

Point mutations in ADA deficiency. While ADA has been isolated from at least ten different mammalian sources, all of the purified enzymes are similar, especially in terms of their substrate specificity and activity and sensitivity to inhibitions by various compounds. Although the amino acid sequence of the 363 residues of human ADA is 11 residues longer than the murine enzyme, there are no gaps in the superimposed sequences of both forms (*30*. The superimposed sequences indicate that the extra residues are all confined to the COOH-terminal end of the polypeptide which, on basis of the murine ADA structure (Fig. 1), would be found near the NH_2-terminal end of the β barrel, a long distance to the active site. The human and murine ADA's also show excellent sequence similarity: 83 percent of the superimposed residues have identical side chains. Presumably the amino acid differences, which are mostly of conservative nature and located near the protein surface, do not affect activity. Finally, the residues directly or indirectly associated with the binding site of the murine ADA superimposed with identical residues in the human ADA sequence.

Inherited deficiency of the ADA accounts for about one-third of the cases of SCID in children (*1*). The sequences of eight mutant ADA complementary DNA's from six cell lines derived from patients with ADA deficiency have been reported (*35–39*) (Table 3). The locations of the residues that undergo point mutations in the primary and tertiary structures of ADA and in relation to the bound HDPR and zinc are listed in Table 3 and shown in Fig. 5. These locations in normal human ADA would have conformations essentially identical to those found in the murine ADA structure, thus enabling us to understand at the molecular level the effect of the point mutations. The residues in the human ADA that undergo point mutations are identical to those in the murine ADA. They are also located in long continuous segments of superposed murine and human ADA sequences with 90 to 93 percent identical residues: Lys^{80} and Arg^{101} are found in a segment of residues from 61 to 133, Arg^{211} in segment 204 to 252, and Pro^{297}, Leu^{304}, and Ala^{329} in segment 288 to 345.

As Arg^{101}, Arg^{211}, Pro^{297}, and Leu^{304} are in close proximity to the active site pocket or to peptide segments that deploy active site residues, including those coordinating the zinc, the loss of activity caused by single mutation of these residues in all five ADA-deficient cell lines can be attributed to structural changes that affect the site. With the exception of Arg^{211}, which is partially exposed to the solvent, all of these residues are buried inside the enzyme. Arg^{101}, which is located underneath the active site pocket and involved in salt linkages with Asp^{181} and Glu^{260}, abuts the three His residues that coordinate the zinc. The mutation of Arg^{211}, which is salt-linked with Glu^{234}, to a less bulkier His residue occurs only two residues away from His^{214}, which participates in coordinating the zinc.

Both Pro^{297} and Leu^{304} reside in a segment (residues 288 to 312) that shows complete sequence identity in both human and murine ADA. Besides being in a hairpin turn that connects β8 to α8, Pro^{297} is preceded by the active site residues Asp^{295} and Asp^{296} located at

Table 3. Locations in the structure of point mutations in ADA-deficient cell lines.

Mutant cell lines	Mutations	Location in the structure		
		Secondary structure	Distance to HDPR (Å)*	Distance to zinc (Å)*
GM2471 (*35*)	Lys_{80}→Arg	α1	15.6	21.1
	Leu^{304}→Arg	First turn of α8	13.5	12.8
GM2606 (*36*)	Arg^{101}→Trp	β2	4.9	4.9
	Arg^{211}→His	β5	14.8	13.8
GM2756 (*37*)	Arg^{211}→His	β5	14.8	13.8
	Ala^{329}→Val	Helix H4†	16.7	15.1
GM1715 (*38*)	Arg^{101}→Gln	β2	4.9	4.9
GM6142 (*39*)	Pro^{297}→Gln	Hairpin loop between β8 and α8	8.3	9.1
GM2825A (*36, 37*)	Ala^{329}→Val	Helix H4	16.7	15.1
	Deletion, residues 74 to 121	α1 and β2		

*Closest distance between the residue in the wild-type ADA and HDPR and the zinc ion. †Secondary structure other than those of the $(\alpha/\beta)_8$ barrel: β1-H1-H2-H3-α1 and α8-H4-H5, where H represents additional helices.

the COOH-terminal end of β8. Leu^{304} is associated with the binding site by contacting a segment of β8 (residues 293 to 296), which not only forms part of active site pocket but also deploys the two Asp residues in the site. Consequently, a mutation of Leu^{304} to Arg would not only transform a nonpolar residue lodged in a hydrophobic environment to a positively charged residue but also impinge on the active site due to a bulkier Arg side chain. Leu^{304} is also three residues from Phe^{300}, which makes van der Waals contact with the active site Asp^{296}.

Analysis in vivo of the two mutant alleles of the GM2471 cell line indicated that, whereas the very conservative Lys^{90} to Arg mutation does not affect enzyme activity, the Leu^{304} to Arg proved deleterious (*35*). Lys^{80} is a peripheral residue located in the first helix (α1) of the barrel, a long distance away from the active site pocket or from any of the segments lining the pocket. The structural basis for the deleterious effect of the Leu^{304} to Arg mutation has been presented above.

Because of the highly conservative mutation of Ala^{329} to Val in one allele of GM2756 and GM2825A and the very remote location of the residue relative to HDPR and zinc, it is less clear how the mutation could lead to the loss of activity. We note, however, that Ala^{329} is within van der Waals distance of the NH_2-terminal end of β1 bearing His^{15} and His^{17}, which coordinate the zinc, and Asp^{19}, which hydrogen bonds the ribose. His^{17} further participates in hydrogen bonding the ribose. The mutation could cause a misalignment of these essential residues.

The mutation in the other allele of GM2825A eliminates exon 4 from the mature messenger RNA and results in the deletion of a 48-residue segment (amino acids 74 to 121). The deleted segment corresponds to α1 and β2 of the ADA structure. The β2 strand forms part of the wall of the active site cavity.

Many of the point mutations thus far examined affect residues lodged in the β strands. No point mutations of residues directly associated with substrate binding and catalysis have been observed. Since the active site pocket, with a bound zinc, is lined by parts of the β strands, it is likely that any mutation that causes a misalignment of the β strands would have a deleterious effect on activity.

Knowledge of the three-dimensional structure of the adenosine deaminase complexed with a transition-state analog has led to a considerable new molecular understanding of the catalytic mechanism of the enzyme and the loss of function caused by point mutations associated with SCID. The previously undetected zinc cofactor is a key element not only in the catalysis but also in correlating many of the mutational effects. The requirement of zinc for ADA is of further interest as zinc deficiency is a major cause of reduced immune function (*40*), possibly as a mimic of ADA deficiency. The structure has important implications for understanding other related nucleotide aminohydrolases with specificities for adenosine monophosphate, guanosine, and cytidine. Our results pave the way for the determination of the structures of mutants, some mimicking those related to ADA deficiency and others probing structure-function relations, generated by site-directed mutagenesis and of complexes with other inhibitors and analogs. We have also obtained crystals of ADA in the presence of the analogs 2′-deoxycoformycin (8*R* and 8*S* Forms) and *erythro*-9-(2-hydroxyl-3-nonyl)adenine and several aromatic compounds (such as rifampicin, phenylbutazone, medazepam, acetaminophen, and dipyridamole) having a considerable range of therapeutic uses. There are at least three dozen known ligands, with diverse types and potencies, to ADA.

REFERENCES AND NOTES

1. N. M. Kredich and M. S. Hershfield, in *The Metabolic Basis of Inherited Disease*, C. R. Scrivner *et al.*, Eds. (McGraw-Hill, New York, ed. 6, 1989), pp. 1045–1075; D. W. Martin and E. W. Gelfand, *Annu. Rev. Biochem.* **50**, 845 (1981).
2. M. J. Cowan, R. O. Brady, K. J. Widder, *Proc. Natl. Acad. Sci. U.S.A.* **83**, 1089 (1983); T. E. Gan, P. E. Dadonna, B. S. Mitchel, *Blood* **69**, 1376 (1987); H. Kanno *et al.*, *Jpn. J. Exp. Med.* **58**, 1 (1988); J. A. Renouf *et al.*, *Clin. Chem.* **35**, 1478 (1989).
3. P. C. Lee, *Dev. Biol.* **31**, 227 (1973); J. M. Chinksy *et al.*, *Differentiation* **42**, 172 (1990).
4. L. Hong *et al.*, *Biol. Reprod.* **44**, 83 (1991).
5. H. McIlwain, in *Central Nervous System Studies on Metabolic Regulation and Function*, E. Genazzari and H. Herken, Eds. (Springer-Verlag, New York, 1983), pp. 3–11; D. Ashton *et al.*, *Eur. J. Pharmacol.* **142**, 403 (1987); D. D. Dawicki, K. C. Agarwal, R. E. Parks, Jr., *Biochem. Pharmacol.* **37**, 621 (1988).
6. R. I. Glazer, *Cancer Chemother. Pharmacol.* **4**, 227 (1980); R. P. Agarwal, *Pharmacol. Ther.* **17**, 399 (1982).
7. L. Frick, J. P. M. Neela, R. Wolfenden, *Bioorg. Chem.* **15**, 100 (1987).
8. C. L. Zielke and C. H. Suelter, *The Enzymes* **4**, 47 (1971).
9. R. Wolfenden, D. F. Wentworth, G. N. Mitchell, *Biochemistry* **16**, 5071 (1969).
10. D. K. Wilson, F. B. Rudolph, M. L. Harrison, R. E. Kellems, F. A. Quiocho, *J. Mol. Biol.* **200**, 613 (1988).
11. M. L. Harrison, D. E. Ingolia, R. E. Kellems, F. B. Rudolph, unpublished data.
12. B. C. Wang, *Methods Enzymol.* **115**, 90 (1985).
13. C. Y. Yeung *et al.*, *J. Biol. Chem.* **260**, 10299 (1985).
14. A. T. Brünger, J. Kuriyan, M. Karplus, *Science* **235**, 458 (1987).
15. A complete description of the structure determination and the refined atomic model will be published separately (D. K. Wilson, F. B. Rudolph, F. A. Quiocho, in preparation).
16. G. K. Farber and G. A. Petsko, *Trends Biochem. Sci.* **15**, 228 (1990).
17. R. Wolfenden, J. Kaufman, J. B. Macon, *Biochemistry* **8**, 2412 (1969); C. Frieden, L. C. Kurz, H. R. Gilbert, *ibid.* **19**, 1616 (1980).
18. L. C. Kurz and C. Frieden, *ibid.* **26**, 8450 (1987).
19. W. Jones, L. C. Kurz, R. Wolfenden, *ibid.* **28**, 12242 (1989); W. M. Kati and R. Wolfenden, *Science* **243**, 1591 (1990).
20. B. F. Cooper, F. A. Quiocho, F. B. Rudolph, unpublished data.
21. B. K. Lee and F. M. Richards, *J. Mol. Biol.* **55**, 379 (1971).
22. E. Lolis and G. A. Petsko, *Annu. Rev. Biochem.* **59**, 597 (1990).
23. M. Ikehara and T. Fukui, *Biochim. Biophys. Acta* **338**, 512 (1974).
24. A. Hampton, P. J. Harper, T. Sasaki, *Biochemistry* **11**, 4736 (1972).
25. T. Sawa *et al.*, *J. Antibiot. (Tokyo). Ser. A* **20**, 317 (1967); P. W. K. Woo *et al.*, *J. Heterocycl. Chem.* **11**, 641 (1974); S. Cha, R. P. Agarwal, R. E. Parks, Jr., *Biochem. Pharmacol.* **24**, 2187 (1975).
26. V. L. Schramm and D. C. Baker, *Biochemistry* **24**, 641 (1985).
27. D. M. Miller III, J. S. Olson, J. W. Pflugrath, F. A. Quiocho, *J. Biol. Chem.* **258**, 13665 (1983); N. K. Vyas, M. N. Vyas, F. A. Quiocho, *Science* **242**, 1290 (1988); F. A. Quiocho, D. K. Wilson, N. K. Vyas, *Nature* **320**, 404 (1989).
28. D. W. Christianson and W. N. Lipscomb, *Acc. Chem. Res.* **22**, 62 (1989).
29. B. W. Matthews, *ibid.* **21**, 333 (1988).
30. Z. Chang, P. Nygaard, A. C. Chinault, R. E. Kellems, *Biochemistry* **30**, 2273 (1991).
31. R. Wolfenden, T. K. Sharpless, R. Allan, *J. Biol. Chem.* **242**, 977 (1967); B. A. Orsi, H. McFerran, A. Hill, A. Bingham, *Biochemistry* **11**, 3386 (1972).
32. M. H. Maquire and M. K. Sims, *Eur. J. Biochem.* **23**, 22 (1971); L. C. Kurz and C. Frieden, *Biochemistry* **22**, 382 (1983); P. M. Weiss, P. F. Cook, J. D. Hermes, W. W. Cleland, *ibid.* **26**, 7378 (1987).
33. B. Evans and R. Wolfenden, *Biochemistry* **12**, 392 (1973).
34. A. L. Akeson, D. A. Wigginton, J. J. Hutton, *J. Cell. Biochem.* **39**, 217 (1989).
35. D. Valerio *et al.*, *EMBO J.* **5**, 113 (1986).
36. A. L. Akeson *et al.*, *J. Biol. Chem.* **263**, 16291 (1988).
37. A. L. Akeson *et al.*, *Proc. Natl. Acad. Sci. U.S.A.* **84**, 5947 (1987).
38. D. T. Bonthron, A. F. Markham, D. Ginsburg, S. H. Orkin, *J. Clin. Invest.* **76**, 894 (1985).
39. R. Hirschhorn, S. Tzall, A. Ellebongen, S. H. Orkin, *ibid.* **83**, 497 (1989).
40. R. L. Gross and P. M. Newberne, *Physiol. Rev.* **60**, 188 (1980).
41. J. S. Sack, *J. Mol. Graphics* **6**, 224 (1988); M. Carson, *ibid.* **5**, 103 (1987).

42. We thank T. Reynolds for making some of the figures and D. Giedroc and H. W. Qui for the atomic absorption analysis of zinc. Supported in part by grants from the National Institutes of Health (grant CA14030) and the Welch Foundation (grant C-1041) to F.B.R. and the Keck Foundation to F.A.Q.F.A.Q. dedicates this paper to F. M. Richards and D. C. Phillips on the occasions of their reaching a milestone.

11 February 1991; accepted 5 April 1991